Heliyon 5 (2019) e01968

Contents lists available at ScienceDirect

Heliyon

journal homepage: www.heliyon.com

Synthesis, characterization and biological activities of imidazo[1,2-a] pyridine based gold(III) metal complexes

Darshana A. Kanthecha, Bhupesh S. Bhatt, Mohan N. Patel *

Department of Chemistry, Sardar Patel University, Vallabh Vidyanagar, 388 120, Gujarat, India

ARTICLE INFO

Keywords:
Inorganic chemistry
Materials chemistry
Organic chemistry
Pharmaceutical chemistry
Imidazo[1,2-a]pyridine
A549 (Lung adenocarcinoma) cell line
Genomic DNA
Cellular level cytotoxicity
Antibacterial activity

ABSTRACT

Five imidazo [1,2-*a*]pyridine derivatives and their Au(III) complexes were synthesized. The compounds were characterized by ^{1}H-NMR, ^{13}C-NMR, IR, mass, UV-visible, elemental analysis, conductivity and magnetic measurement studies. All the compounds were screened for diverse biological activities to check the effect of coordination of Au(III) with imidazo [1,2-*a*]pyridine heterocycles. The DNA interaction ability of compounds were studied as the change in absorption maxima and position of HS-DNA in presence of compounds and viscosity measurement due to change in DNA length under the influence of compounds. The computational insight of compound-DNA interaction was taken in docking study. All the results suggest intercalation mode of binding. The cellular level cytotoxic nature of compounds was evaluated using trypan blue dye staining of dead cell in cell viability assay. The smearing of DNA was observed, while DNA extracted from *S. pombe* cells in presence of complexes was subjected to gel electrophoresis, which shows their toxic effect on DNA. The complexes were evaluated for cytotoxicity on human A549 (Lung adenocarcinoma) cell line by MTT assay (IC_{50} values). The *in vitro* cytotoxicity in terms of LC_{50} value was checked on a simple zoological organism, brine shrimp.

1. Introduction

DNA is a clinically important molecular target of anticancer agents, which includes DNA intercalators, DNA synthesis inhibitors, transcription regulators and enzyme inhibitors. However, DNA is a non-specific target for traditional chemotherapeutic drugs, and so newer strategies have been developing in designing more selective, target specific and less toxic chemotherapeutic agents [1]. The drug can interact with DNA either through controlling enzymes involved in transcription or directly with the double helix parts of DNA, mainly phosphate backbone and nucleobases.

Metal ions are essential to many biological and chemical processes and their properties can be applied in designing new anticancer drugs [2]. After the fortuitous discovery of most important and widely used chemotherapeutic agent cisplatin by Barnett Rosenberg [3], medicinal inorganic chemistry has been revolutionized and significant efforts have been made to identify newer metal based cytotoxic agents [4]. So most of the research has been focused on designing cisplatin analogue anticancer agents [5]. However, the administration of platinum based drugs have limitations of adverse side effects and acquired or intrinsic drug resistance [6], and hence there is a necessity of newer chemotherapeutic agents which can replicate the effectiveness of cisplatin, and can overcome its side effects. The cytotoxic activity of different transition metal complexes have been researched [7], and within this field, significant approaches have been made in exploring the cytotoxic activity of gold complexes [8], and their ability to interact with DNA [2c, 9].

The coordination of small organic molecules often produces a significant effect on their biological activities [10]. Within this context, we synthesized heterocyclic imidazo [1,2-*a*]pyridine derivatives owing to their huge biological and medicinal applications [11], and their gold (III) complexes. In this article, we have attempted to explore the combined biological effect of gold (III) metal ion and imidazole based molecules, which can be useful for novel anticancer drug design and development strategies.

2. Result and discussion

2.1. Spectral and analytical characterization

The reaction scheme for the synthesis of all compounds is provided in Scheme 1. The ^{1}H-NMR, ^{13}C-NMR and IR spectra of L^{1} and complex-I are given in Fig. 1 and Fig. 2, respectively.

* Corresponding author.
E-mail address: jeenen@gmail.com (M.N. Patel).

https://doi.org/10.1016/j.heliyon.2019.e01968
Received 16 November 2018; Received in revised form 7 May 2019; Accepted 14 June 2019

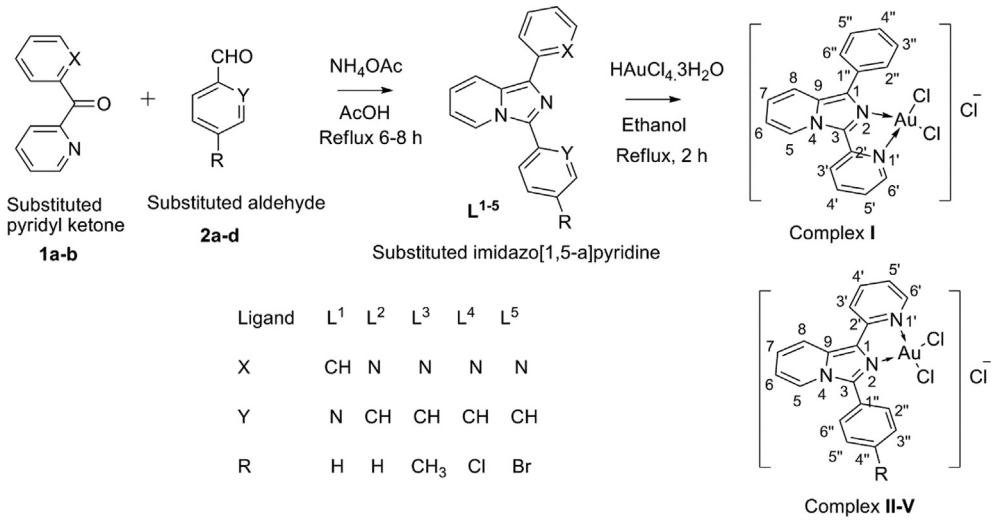

Scheme 1. Reaction scheme for the synthesis of compounds.

The NMR and IR spectral data of imidazo [1,2-*a*]pyridine derivatives and gold (III) complexes are provided in the experimental section. There is large downfield shift observed for the protons ($H_{3'}$, $H_{6'}$ = 8.510, 8.677 δ ppm) of pyridyl ring of imidazo [1,2-*a*]pyridine heterocycle after complexation with gold (III) metal ion in complex-I ($H_{3'}$, $H_{6'}$ = 8.515, 8.683 δ ppm) in ^{1}H-NMR spectra. Such downfield shift is also observed in ^{13}C-NMR spectra of L^1 and complex-I, particularly for quaternary C_1 (129.05 for L^1 and 132.07 for I) and $C_{2'}$ (149.57 for L^1 and 155.01 for I). These clearly indicate the nearby N_2 and $N_{1'}$ as the coordinating atoms. Infrared spectra of the imidazo [1,2-*a*]pyridine heterocycles show intense band for ν(C=N) at 1589 cm^{-1}, which is shifted to 1650 cm^{-1} in complex-I, which suggests N as the coordinating atom. Also an additional band at 516 cm^{-1} appears in IR spectra, which is the characteristic band of Au–N stretching. Such spectral shifts are also observed for all the compounds. The mass spectrum of complex-I shows expected m/z values for molecular ion peak and peaks of corresponding fragments of complex-I (Fig. 3).

The μ_{eff} value obtained by magnetic moments measurement at room temperature of gold (III) complexes were observed zero B.M, suggests all paired electron in the low-spin 5d^8 configuration of gold complexes with the gold ion in +3 oxidation state. The electronic spectra of complex-1 in DMSO exhibit intra-ligand charge transfer band (π–π*) and MLCT band (n–π*) at ~300 nm and ~370 nm, respectively. The molar conductivity value of the gold (III) complexes are in the range of 91–101 cm^2 Ω^{-1} mol^{-1} at room temperature, which suggests the electrolytic nature of metal complexes having one counter ion outside the coordination sphere. So, we conclude that all synthesized gold (III) complexes having chlorine as counterion and square-planar geometry.

2.2. Antibacterial activity

The adaptation of bacteria towards the lethal effect of antibiotic has become one of the biggest threats to global health. A growing number of infections (pneumonia, tuberculosis, gonorrhea, salmonellosis) are becoming harder to treat due to the emerging problem of antibiotic resistance by bacteria. The development of resistance towards antibiotic by bacteria can be achieved through either neutralizing the drug or through a morphological change in the outer layer by which a drug can be pumped back outside of the bacteria. It is a well-known fact that chelation of organic molecule with metal ion results in a drastic increase in the antibacterial efficacy [12]. Hence, we evaluated the antibacterial activity of metal complexes against three Gram-negative bacterial strains: *E. coli, S. marcescens* and *P. aeruginosa*; and against two Gram positive bacterial strains: *B. subtilis* and *S. aureus* using the broth dilution method. From the data (Fig. 4 and Table 1), it can be concluded that all the metal complexes (62–102 μM) are more active than imidazo [1,2-*a*]pyridine derivatives (220–320 μM) against all the tested pathogens, but the activity is seldom enough for application of complexes as antibacterial agents.

2.3. DNA interaction study using UV-visible absorption spectroscopy

DNA is an important target of many therapeutic agents for exerting their efficacy. Therapeutic agents can target DNA in different ways either through inhibiting topoisomerase enzyme to inhibit bacterial replication as in the case of antibacterial agents or can directly link with the DNA to inhibit the uncontrolled cell growth as in the case of anticancer agents. The DNA susceptibility test can explore new ways of designing more effective therapeutic agents that can inhibit the growth of tumor cells or inhibit the multiplication of bacteria. UV–visible absorption spectroscopy is a useful technique to probe compound–DNA interaction in which the change in absorption maxima λ_{max} and intensity due to conformational changes in DNA structure caused by interaction with any compound is quantified [13]. The magnitude of any change directs the strength and mode of interaction. Intercalative mode of binding produces hypochromism with a redshift, due to the interaction between the pi antibonding orbital (π*) of the intercalated molecule and the pi bonding orbital (π) of DNA base pairs [14]. The change in DNA conformation due to electrostatic interaction of ionic molecule results in hyperchromism for both DNA and the interacting molecule. The DNA-compound adducts formation at groove region results in hyperchromism with no or very little redshift, which is believed to be due to the interaction between electronic states of interacting molecules and nitrogenous bases of DNA [15].

The characteristic absorption peak of metal complexes due to π-π* electronic transition of ligands (imidazo [1,2-*a*]pyridine derivatives) at ~280 nm was taken as the reference to study the interaction. As shown in the Fig. 5, the characteristic absorption peak of DNA due to π–π transition of DNA base pairs is shifted from 260 nm and appeared along with the wavelength of ligand molecule, which clearly indicates a significant perturbation in the DNA conformation due to interaction with Au(III) complexes. The UV–visible spectra of complex-I (5 μM) with gradual addition of HS-DNA (0–100 μM) is shown in Fig. 5. As is evident from the spectra, with increasing concentration of complex-I, the absorbance of DNA at 280 nm decreases (hypochromism) with large redshift. Similar trends were observed for DNA interaction studies of all ligands and metal complexes, which suggests the significant structural changes in DNA due to intercalation of compounds in between the stacks of DNA base pairs.

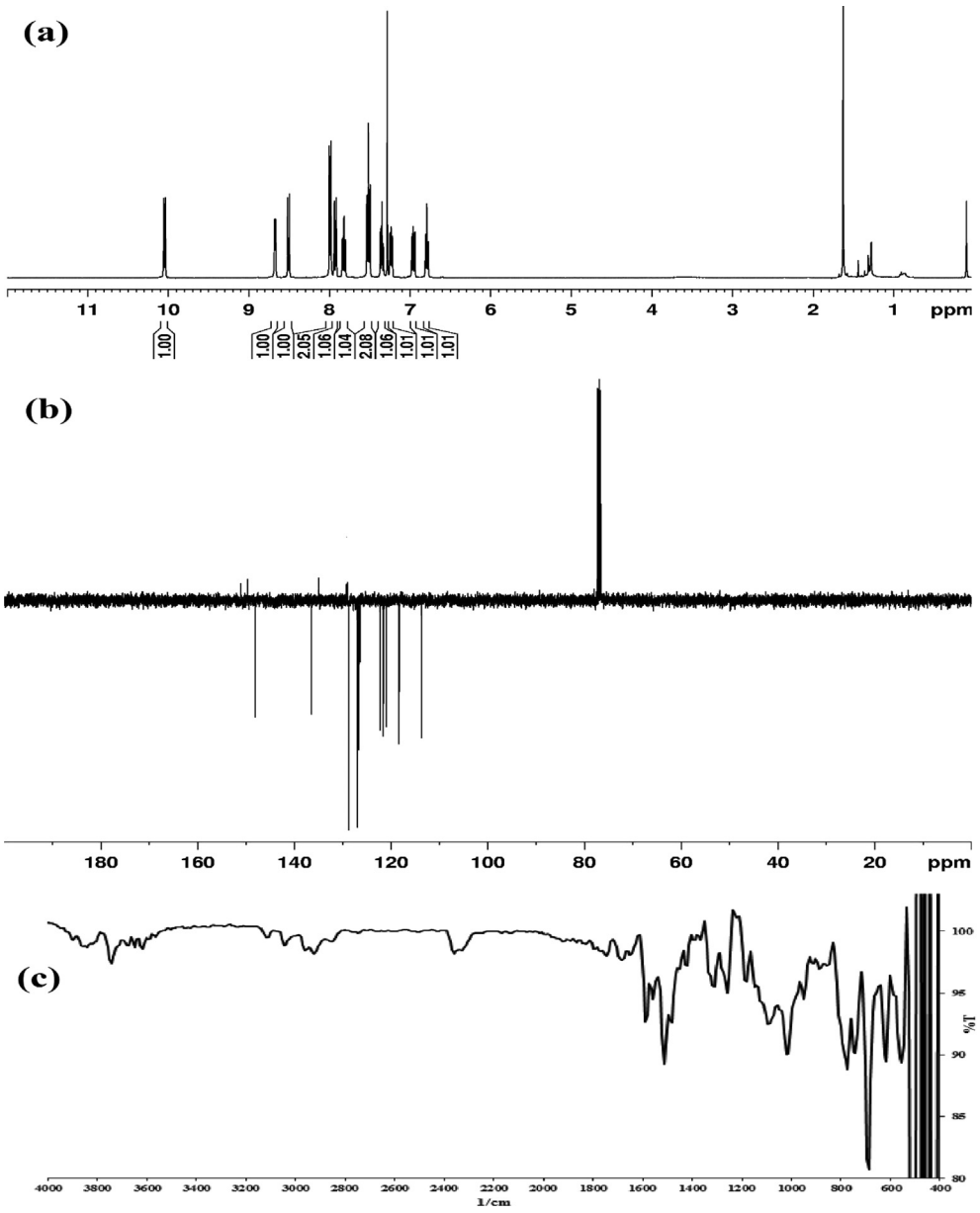

Fig. 1. (a) ^{1}H-NMR, (b) ^{13}C-NMR and (c) IR spectra of L^{1}.

The evaluation of quantitative binding strength of compounds with DNA in terms of K_b value reveal the higher binding strength of metal complexes ($K_b = 0.9 \times 10^5$–1.6×10^5) than ligand molecules ($K_b = 4 \times 10^4$–5×10^4), which again emphasize the role of metal ion in increasing the affinity of ligands towards DNA. The highest binding strength is observed for complex-4 having Cl atom as a substituent at ancillary ligand, which may be attributed to its smaller size and its ability to polarize DNA base pairs. Hence, we may also conclude that compound-DNA complex is stabilized through van der Walls interactions. The K_b value of all the compounds is shown in Table 2. The observed K_b values of complexes are comparable to higher than reported N,N-donor ligand based DNA intercalator Au(III) complexes ($K_b = 1.3 \times 10^5$–4.4×10^5) [9b,9c], but higher than reported dithiocarbamate ligand based phosphanegold(I) complexes ($K_b = 3.9 \times 10^4$–8.5×10^4), where interaction is electrostatic [16]. The complexes show similar biological potency with standard DNA intercalating drug, doxorubicin ($K_b = 1.3 \times 10^5$ M^{-1} in 10% serum at 37 °C) [17], but lower potency than classical intercalator EtBr ($K_b = 7 \times 10^7$ M^{-1}) [18].

2.4. DNA interaction study using viscosity measurement

Measurement of viscosity is a simple, complementary and excellent method to know the mode of binding of metal complexes to DNA. The DNA helix lengthens, as the base pairs are separated to accommodate the bound ligand for the intercalation of the molecule, leading to an increasing in DNA viscosity. Viscosity measurement is thus a suitable method to detect such changes and, in the absence of crystallographic structural data, it is an essential evidence to support an intercalation model. In contrast, non-classical intercalation of ligands could bend the DNA helix, reduce its effective length and in turn, its viscosity. The relative viscosity of DNA solution (200 μM) in presence of all the imidazo [1,2-*a*]pyridine derivatives and Au(III) complexes (0–40 μM) increases, which suggests intercalation mode of binding as suggested by UV-visible absorption titration study. The magnitude of change in relative viscosity in presence of complexes is higher than imidazo [1,2-*a*]pyridine derivatives, due to increase in binding strength of imidazo [1,2-*a*]pyridine derivatives upon complexation with Au(III) metal ion, but change in relative viscosity of metal complexes are lower than classical intercalator

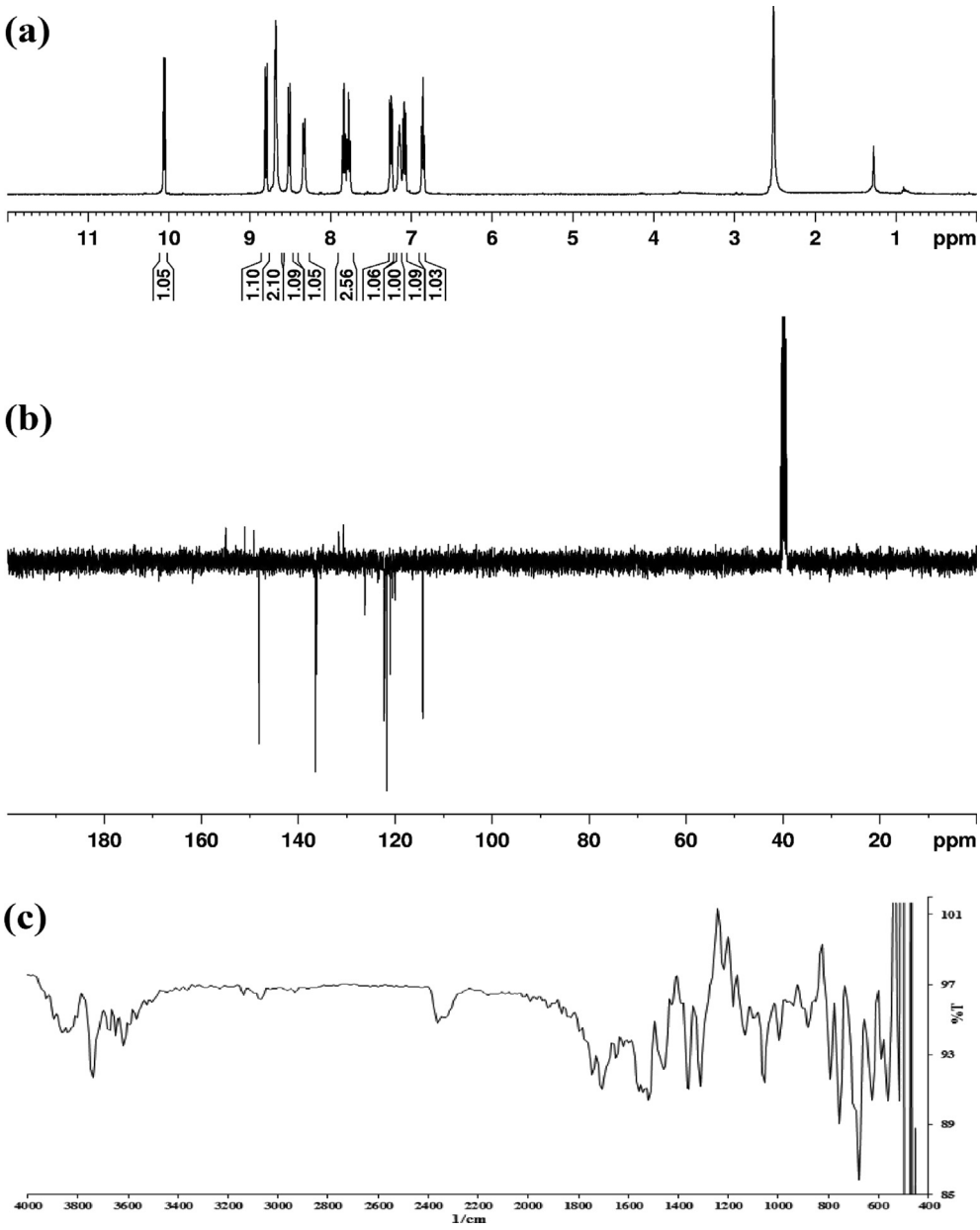

Fig. 2. (a) ^{1}H-NMR, (b) ^{13}C-NMR and (c) IR spectra of complex-I.

EtBr (Fig. 6). The results are also supported by previous studies of DNA interaction of Au (III) complexes [9b].

2.5. Molecular docking

The theoretical binding behavior of the synthesized compounds toward DNA was explored on B-DNA duplex of sequence (1 BNA: 5′-D(*CP*GP*CP*GP*AP*TP*TP*CP*GP*CP*G)-3′). The sterically acceptable DNA-compound conformation was taken to predict the binding affinity and binding site. The minimum energy docked pose suggest minor groove with a rich G-C base pair as the first interaction site of metal complexes as shown in Fig. 7, followed by the intercalation of complexes in between the stacks of DNA base pairs as suggested by UV-Vis. absorption study and viscosity measurement. The binding energy values are shown in Table 2. The negative values of the binding free energy of the docked complexes suggest reasonably binding of compounds with DNA.

2.6. In vitro cytotoxicity

Brine shrimp lethality bioassay is a simple, cost-effective and commonly used preliminary toxicity screening of bioactive compound of either natural or synthetic origin on the laboratory cultured larvae (nauplii). This lethality bioassay was employed as a bioassay guide for active cytotoxic and antitumor agents in 1982 [19]. In this method, the nauplii were exposed to different concentrations of complexes (2–20 μg/mL) for 24 h. The number of motile nauplii was calculated for the effectiveness of the compounds, and LC_{50} value was calculated as a measurement of cytotoxic nature of compounds, from the graph drawn between % mortality and the log of compound concentration (Fig. 8). The LC_{50} values (Table 2) of complexes are obtained in the range of 5.12–7.94 μg/mL, while LC_{50} values of imidazo [1,2-*a*]pyridine derivatives are 20.07–27.82 μg/mL. The results suggest that metal complexes are better cytotoxic agents than imidazo [1,2-*a*]pyridine derivatives, also that the bioactivity of imidazo [1,2-*a*]pyridine derivatives increase upon complexation with the metal ion.

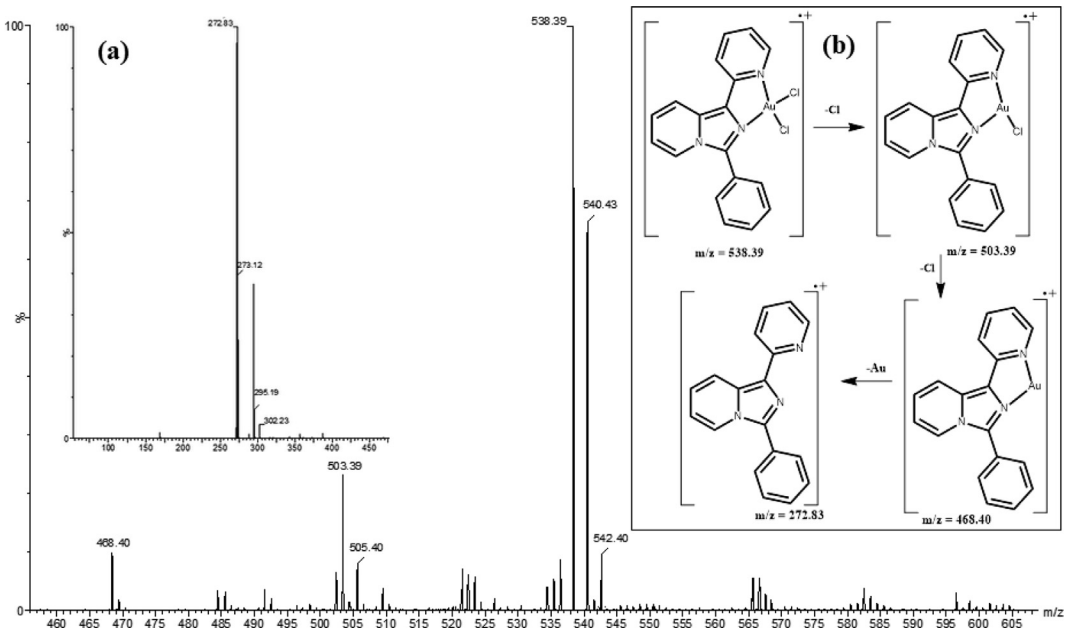

Fig. 3. (a) Mass spectrum and (b) fragmentation pattern of complex-I.

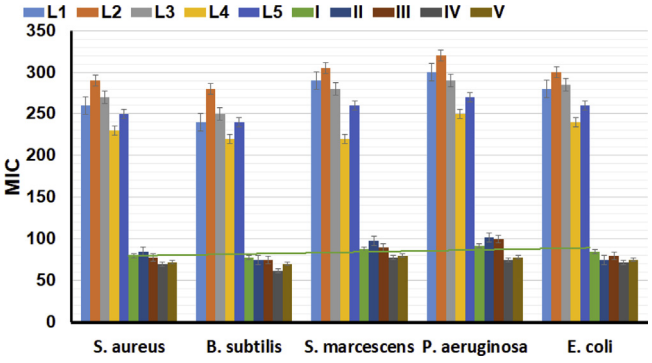

Fig. 4. Graphical representation of *in vitro* antibacterial activity of compounds.

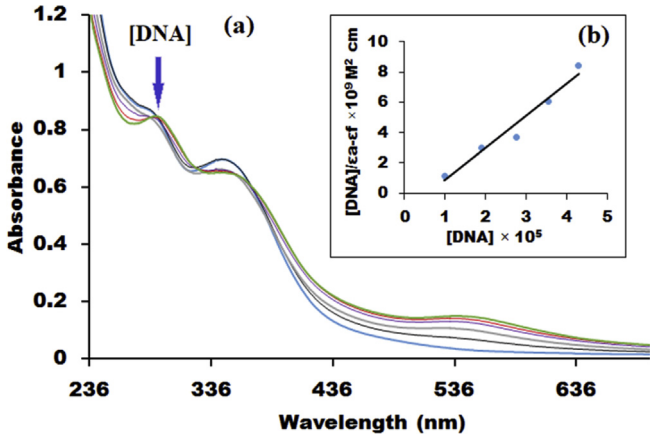

Fig. 5. (a) Absorption spectra upon addition of HS DNA (0–100 μM) to the solution of complex-I (5 μM) after incubating for 10 min at room temperature in phosphate buffer (Na_2HPO_4/NaH_2PO_4, pH = 7.2). (b) Inset: plot of [DNA]/($\varepsilon_a - \varepsilon_f$) vs. [DNA].

Table 1
Antibacterial activity data in terms of MIC (μM) of imidazo [1,2-a]pyridine derivatives and Au(III) complexes.

Compound	Gram (+ve)		Gram (-ve)		
	S. aureus	*B. subtilis*	*S. marcescens*	*P. aeruginosa*	*E. coli*
L^1	260	240	290	300	280
L^2	290	280	305	320	300
L^3	270	250	280	290	285
L^4	230	220	220	250	240
L^5	250	240	260	270	260
I	80	78	88	92	85
II	85	75	98	102	75
III	78	75	90	100	80
IV	70	62	78	75	72
V	72	70	80	78	75

2.7. Cellular level cytotoxicity

The effect of concentration and complexation on the cellular level cytotoxicity of imidazo [1,2-*a*]pyridine derivatives on the eukaryotic *Schizosaccharomyces pombe* (*S. pombe*) cells were carried out using a trypan blue assay. The *S. pombe* cells were exposed to different concentration of imidazo [1,2-*a*]pyridine derivatives and their Au(III) complexes (2–10 μg/mL) for 17 h, followed by staining with trypan blue dye.

Table 2
Biological activities data of ligands and Au(III) complexes.

Compounds	LC_{50} (μg/mL)*	K_b (10^5 M^{-1})#	Binding Energy (kJ mol^{-1})*#	IC_{50} (μg/mL)**#
L^1	26.21	0.5	-232.8	-
L^2	27.82	0.4	-225.9	-
L^3	24.15	0.4	-233.7	-
L^4	23.27	0.5	-241.9	-
L^5	20.07	0.4	-240.8	-
Complex-I	6.49	1.0	-289.98	141.79
Complex-II	7.94	0.9	-303.17	273.86
Complex-III	6.03	1.1	-309.57	214.57
Complex-IV	5.31	1.6	-306.54	117.53
Complex-V	5.12	1.1	-310.10	112.14

* As evaluated by brine shrimp lethality bioassay.
\# As evaluated by UV-visible absorption titration between DNA and compounds.
*# As evaluated by molecular docking study.
**# As evaluated by MTT assay.

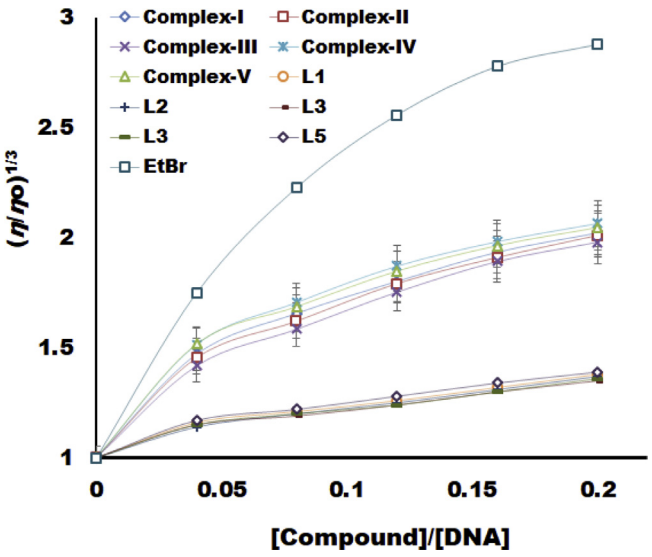

Fig. 6. Viscosity measurement graph of DNA-compounds interaction.

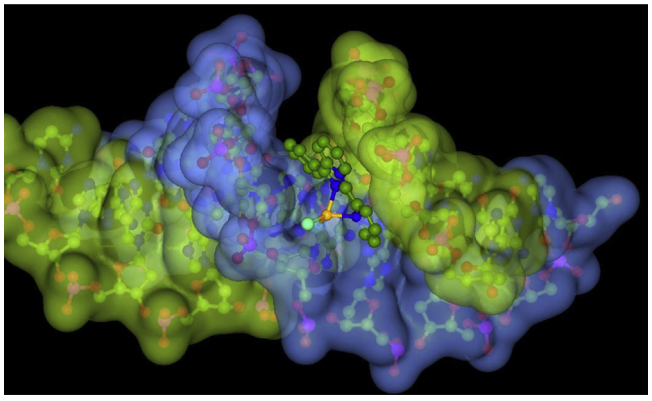

Fig. 7. Representative image of molecular docking of complex-I with B-DNA.

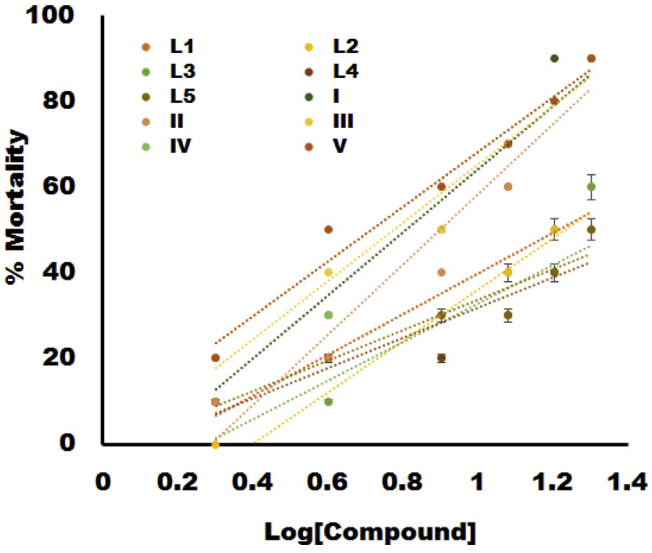

Fig. 8. Linear plot of % mortality of brine shrimp vs the logarithm of compounds concentration.

The dye can be penetrated through the dead cell and will appear blue [20]. The graphical representation of i*n vivo* cytotoxicity of imidazo [1,2-*a*]pyridine derivatives, Au(III) complex, cisplatin and transplatin (standard drug) are shown in Fig. 9. The percentage viability of cells treated with imidazo [1,2-*a*]pyridine derivatives and complexes suggest that the cytotoxicity of imidazo [1,2-*a*]pyridine derivatives increases upon complexation, and also that the percentage viability of cells increases with increase in concentration of all compounds.

2.8. Genotoxicity evaluation by single cell gel electrophoresis

DNA extraction has been carried out from *S. pombe* cells for the study of DNA cleavage by agarose gel electrophoresis [21]. The result shows the effects of the compound on the integrity of DNA. The damage caused by complex on DNA can be seen as DNA smearing due to the toxic nature of the compound, whereas control cell DNA appeared normal as an intact band (Fig. 10). The result suggests complex as a good genotoxic agent. The cellular level toxicity of complex break the DNA from the nucleus. The increase in complex concentration results in an increase in DNA smearing.

2.9. MTT assay

The half inhibitory concentration (IC_{50} values) for the Au(III) complexes with cell proliferation of the A549 (Lung adenocarcinoma) cell line was evaluated by MTT assay from the plot represented in the Fig. 11. In the assay, the complexes-IV and V (Table 2) were appeared as the most potent cytotoxic agents. The potent cytotoxic nature of complexes-IV and V can be attributed to their more lipophilic nature due to presence of electronegative halogen substituents at the ancillary ligands. As shown in cell death analysis (Fig. 11), all complexes efficiently induce cell death in A549 cells within time period of 24 h. Thus, these results indicate that all complexes induce inhibition of cell proliferation in cancer.

3. Conclusion

Five different imidazo [1,2-*a*]pyridine derivatives and their gold (III) complexes were synthesized. The analytical and spectral characterization of complexes show gold metal ion in +3 oxidation state, Cl^- as the counterion and square planar geometry of gold (III) complexes. The biological studies suggest that the potency of imidazo [1,2-*a*]pyridine derivatives improve in presence of metal ion. The DNA binding activities using UV-visible absorption titration indicates intercalation of compounds in between the stacks of DNA base pairs. Similar results were reflected in the relative viscosity measurement. The molecular docking study reveals rich G-*C minor* groove region of DNA as the primary interacting site for compounds, followed by intercalation as suggested in DNA binding studies.

The evaluation of *in vitro* cytotoxicity in term of LC_{50} value and *in vivo* cytotoxicity profile in terms of cell viability assay of compounds revealed that the cytotoxicity of imidazo [1,2-*a*]pyridine derivatives increase upon complexation. The gel electrophoresis of genomic DNA in presence of compounds suggests potent genotoxic nature of compounds. Also in MTT assay, all the complexes show potent cytotoxic nature and induce inhibition of A549 cell proliferation. The antibacterial activity of compounds in terms of MIC reveals that metal complexes have far better antibacterial activity than imidazo [1,2-*a*]pyridine derivatives. So from the above studies, we can conclude that coordination of metal ion has major impact on the biological activities of organic molecules, and this strategy can be utilized for modern approaches of drug discovery.

4. Experimental

4.1. Chemicals and materials

All analytical grade chemicals and solvents were used as commercially received. $HAuCl_43H_2O$ was purchased from S.D. Fine-Chem Ltd. (India.). 2,2-Dipyridylketone, 2-benzoyl pyridine, benzaldehyde, 4-

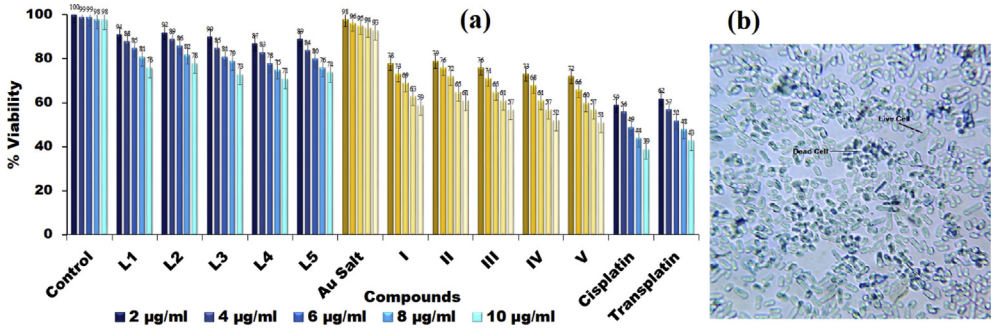

Fig. 9. (a) Cytotoxicity data in terms of % cell viability of imidazo [1,2-a]pyridine derivatives and Au(III) complexes; (b) *S. pombe* cell upon treated with compound observed under the microscope (40x).

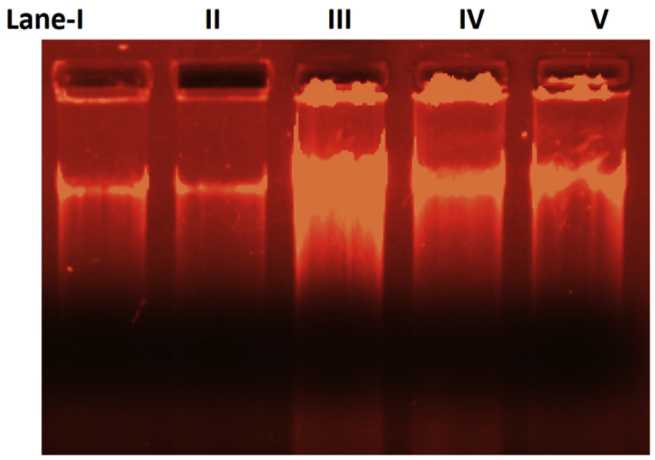

Fig. 10. Photogenic view of cleavage of *S. pombe* DNA (1 μgL^{-1}) with complex-1 using 1% agarose gel containing 0.5 (μgL^{-1}) EtBr; Lane-I: 2 µg/mL complex + DNA + EtBr; Lane-II: 4 µg/mL complex + DNA + EtBr; Lane-III: 6 µg/mL complex + DNA + EtBr; Lane-IV: 8 µg/mL complex + DNA + EtBr; Lane-V: 10 µg/mL complex + DNA + EtBr.

methyl benzaldehyde, 4-bromo benzaldehyde, 4-chloro benzaldehyde, 4-methoxy benzaldehyde, HS-DNA and EDTA were purchased from Sigma Aldrich Chemical Co. (India). Agarose, Luria Broth (LB), ethidium bromide (EtBr), Tris–acetyl–EDTA (TAE) and bromophenol blue were purchased from Himedia (India). Culture for antibacterial activity *Bacillus subtilis (B. subtilis-7193)*, *Staphylococcus aureus (S. aureus-3160)*, *Pseudomonas aeruginosa (P. aeruginosa-1688)*, *Escherichia coli (E. coli-433)* and *Serratia marcescens (S. marcescens-7103)* were purchased from the Institute of Microbial Technology (Chandigarh, India). *S. Pombe* Var. Paul Linder 3360 was obtained from IMTECH, Chandigarh.

4.2. Physical measurements

Elemental analysis of C, H, and N was performed with a model EuroVector EA3000 (for imidazo [1,2-*a*]pyridine derivatives) and Perkin-Elmer 240 (for complex) elemental analyzer. The LC-MS spectra were recorded using Thermo scientific mass spectrophotometer (USA). Bruker Avance spectrophotometer was used for recording ^{1}H NMR (400 MHz) and ^{13}C NMR (100 MHz) spectra. Melting points were determined in open capillaries on hermocal10 melting point apparatus (Analab Scientific Pvt. Ltd, India). The Gouy's method was used for magnetic measurement of metal complexes taking mercury tetrathiocyanatocobaltate (II) as the calibrant ($\chi g = 16.44 \times 10\text{-}6$ cgs units at 20 °C), citizen balance. UV-160A UV-Vis spectrophotometer, Shimadzu, Kyoto (Japan), was used for electronic spectra of metal complexes in the range of 200–800 nm using quarts cell having a path length of 1 cm. Ubbelohde viscometer in viscosity bath having a controllable temperature (25.0 ± 0.5 °C) was used for the study of hydrodynamic chain length. The antibacterial study was carried out by means of laminar air flow cabinet Toshiba, Delhi (India). Alphadigidoctm RT. Version V.4.0.0 PC– Image software, CA (USA) used for the Photo quantization of the DNA cleavage activity.

4.3. Synthesis, spectral and analytical data of imidazo[1,2-a]pyridine derivatives

Synthesis of imidazo [1,2-*a*]pyridine derivatives was carried out by

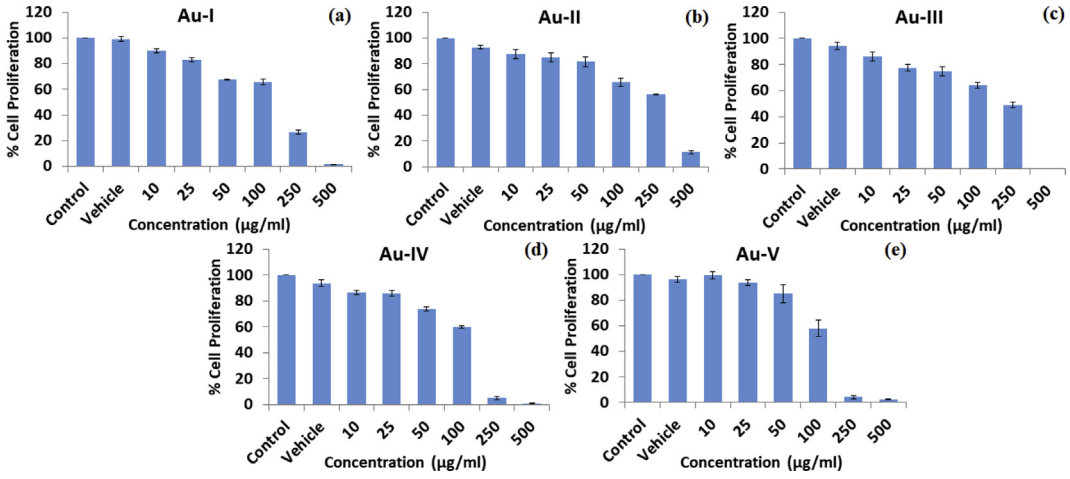

Fig. 11. Evaluation of A549 cell death data by (a) Au–I, (b) Au-II, (c) Au-III, (d) Au-IV and (e) Au–V complexes using MTT assay.

taking a mixture of pyridylketone (5 mmol), substituted benzaldehyde (5 mmol), and NH_4OAC (15 mmol) in 15 mL of glacial acetic acid in a 100 mL round bottom flask equipped with a condenser. The reaction mixture was heated at 80–120 °C under N_2 gas for 6–8 h. Upon checking TLC in an interval of 1 h, when all the reactants were consumed and a spot of the product appears the reaction mixture was cooled to room temperature and then kept the solution under temp 15–20 °C to slow evaporation overnight. The resulting yellow residue was filtered and purified using column chromatography on silica gel by ethyl acetate: hexane (2:8) system as a mobile phase.

4.3.1. 1-Phenyl-3-(pyridin-2-yl)imidazo[1,5-a]pyridine (L^1)

Synthesized using 2-benzoylpyridine with 2-pyridinecarboxaldehyde as given procedure. Colour: yellow, Yield: 58%, mol. wt.: 271.32 g/mol, m. p.: 124.3 °C, Anal. Calc. (%) For $C_{18}H_{13}N_3$: C, 79.68; H, 4.83; N, 15.49 Found (%): C, 79.85; H, 4.72; N, 15.25. ^{1}H NMR (400 MHz, DMSO-d_6) δ/ppm: 6.774–6.811(1H, m, H_6), 6.942–6.983(1H, m, H_7), 7.219–7.253(1H, m, $H_{4''}$), 7.351(1H, t, J = 7.6 Hz, $H_{5'}$), 7.518(2H, t, J = 7.6 Hz, $H_{3'',5''}$), 7.823–7.844(1H, m, $H_{4'}$), 7.930(1H, d, J = 9.2 Hz, H_8), 7.993(2H, dd, J = 0.8, 7.2 Hz, $H_{2'',6''}$), 8.510(1H, d, J = 8.0 Hz, $H_{3'}$), 8.677(1H, dd, J = 0.8, 4.0 Hz, $H_{6'}$), 10.057(1H, d, J = 7.6 Hz, H_5), ^{13}C NMR (100 MHz, DMSO-d_6) δ/ppm: 113.67(CH C_6), 118.37(CH C_8), 120.97(CH $C_{5'}$), 121.63(CH $C_{3'}$), 122.26(CH C_7), 126.39(CH $C_{2'',6''}$), 126.71(CH C_5), 127.00(CH $C_{4''}$), 128.76(CH $C_{3'',5''}$), 129.05($C_{quaternary}$ $C_{1'}$), 129.33($C_{quaternary}$ C_9), 135.03($C_{quaternary}$ $C_{1''}$), 136.55(CH $C_{4'}$), 148.12(CH $C_{6'}$), 149.57($C_{quaternary}$ $C_{2'}$), 151.50($C_{quaternary}$ C_3). FT-IR (400-4000 cm^{-1}): ν(C–H)$_{stretching}$; 3047 cm^{-1}, ν(C=N)$_{stretching}$; 1589 cm^{-1}, ν(C=C)$_{stretching}$; 1512, 1481 cm^{-1}, ν(C–N)$_{stretching}$; 1257 cm^{-1}, Mass (m/z): 272.

4.3.2. 3-Phenyl-1-(pyridin-2-yl)imidazo[1,5-a]pyridine (L^2)

Synthesized using 2,2′-dipyridylketone with benzaldehyde as given procedure. Colour: yellow, Yield: 82%, mol. wt.: 271.32 g/mol, m. p.:108 °C, Anal. Calc. (%) For $C_{18}H_{13}N_3$: C, 79.68; H, 4.83; N, 15.49 Found (%): C, 79.86; H, 4.74; N, 15.26. ^{1}H NMR (400 MHz, DMSO-d_6) δ/ppm: 6.668(1H, t, J = 6.4 Hz, H_6), 6.944(1H, dd, J = 2.8, 6.4 Hz, H_7), 7.104–7.136(1H, m, $H_{4''}$), 7.486(1H, d, J = 7.6 Hz, $H_{5'}$), 7.574(2H, t, J = 8.0 Hz, $H_{3'',5''}$), 7.719–7.762(1H, m, $H_{4'}$), 7.868(2H, d, J = 7.2 Hz, $H_{8,3'}$), 8.279(2H, d, J = 8.4 Hz, $H_{2'',6''}$), 8.658(1H, d, J = 5.2 Hz, H_5), 8.736(1H, d, J = 8.8 Hz, $H_{6'}$). ^{13}C NMR (100 MHz, DMSO-d_6) δ/ppm: 113.91(CH C_6), 119.96(CH C_8), 120.45(CH $C_{5'}$), 121.02(CH $C_{3'}$), 121.62(CH C_7), 121.89(CH $C_{2'',6''}$), 128.41(CH C_5), 128.94(CH $C_{3''}$), 129.05(CH $C_{5''}$), 130.17($C_{quaternary}$ C_9), 130.23($C_{quaternary}$ $C_{1'',3}$), 130.65(CH $C_{4''}$), 136.27(CH $C_{4'}$), 138.06($C_{quaternary}$ C_1), 149.01(CH $C_{6'}$), 155.09($C_{quaternary}$ $C_{2'}$). FT-IR (400-4000 cm^{-1}): ν(C–H)$_{stretching}$; 3055 cm^{-1}, ν(C=N)$_{stretching}$; 1589 cm^{-1}, ν(C=C)$_{stretching}$; 1512, 1473 cm^{-1}, ν(C–N)$_{stretching}$; 1280 cm^{-1}, Mass (m/z): 272.

4.3.3. 1-(Pyridin-2-yl)-3-(p-tolyl)imidazo[1,5-a]pyridine (L^3)

Synthesized using 2,2′-dipyridylketone with p-tolylbenzaldehyde as given procedure. Colour: yellow, Yield: 79%, mol. wt.: 285.35 g/mol, m. p.: 154.7 °C, Anal. Calc. (%) For $C_{19}H_{15}N_3$: C, 79.98; H, 5.30; N, 14.73 Found (%): C, 80.08; H, 5.19; N, 14.73. ^{1}H NMR (400 MHz, DMSO-d_6) δ/ppm: 2.472(3H, s, CH_3), 6.654(1H, t, J = 6.4 Hz, H_6), 6.930 (1H, dd, J = 2.8, 6.4 Hz, H_7), 7.097–7.128(1H, m, $H_{5'}$), 7.378(2H, d, J = 8.0 Hz, $H_{3'',5''}$), 7.713–7.761(3H, m, $H_{3',4',8}$), 8.260(2H, t, J = 7.2 Hz, $H_{2'',6''}$), 8.650(1H, d, J = 4.8 Hz, H_5), 8.711(1H, d, J = 9.2 Hz, $H_{6'}$). ^{13}C NMR (100 MHz, DMSO-d_6) δ/ppm: 21.43(CH_3 $C_{7''}$), 113.74(CH C_6), 119.94(CH C_8), 120.36(CH $C_{5'}$), 120.86(CH $C_{3'}$), 121.68(CH C_7), 121.82(CH $C_{2'',6''}$), 127.27($C_{quaternary}$ $C_{4''}$), 128.32(CH C_5), 129.72(CH $C_{3'',5''}$), 130.09($C_{quaternary}$ C_9), 130.57($C_{quaternary}$ C_3), 136.20(CH $C_{4'}$), 138.26($C_{quaternary}$ $C_{1''}$), 138.95($C_{quaternary}$ C_1), 148.98(CH $C_{6'}$), 155.15($C_{quaternary}$ $C_{2'}$). FT-IR (400-4000 cm^{-1}): ν(C–H)$_{stretching}$; 3024 cm^{-1}, ν(C=N)$_{stretching}$; 1589 cm^{-1}, ν(C=C)$_{stretching}$; 1512, 1481 cm^{-1}, ν(C–N)$_{stretching}$; 1218 cm^{-1}, Mass (m/z): 286.

4.3.4. 3-(4-Chlorophenyl)-1-(pyridin-2-yl)imidazo[1,5-a]pyridine (L^4)

Synthesized using 2,2′-dipyridylketone with p-chlorobenzaldehyde as given procedure. Colour: yellow, Yield: 89%, mol. wt.: 305.77 g/mol, m. p.: 165.01 °C, Anal. Calc. (%) For $C_{18}H_{12}ClN_3$: C, 70.71; H, 3.96; N, 13.74 Found (%): C, 70.71; H, 3.63; N, 13.74. ^{1}H NMR (400 MHz, DMSO-d_6) δ/ppm: 6.709(1H, t, J = 6.0 Hz, H_6), 6.967(1H, dd, J = 3.6, 6.4 Hz, H_7), 7.131(1H, dd, J = 2.0, 4.4 Hz, $H_{5'}$), 7.551(2H, d, J = 8.8 Hz, $H_{3'',5''}$), 7.725–7.770(1H, m, $H_{4'}$), 7.825(2H, d, J = 8.4 Hz, $H_{8,3'}$), 7.242(2H, t, J = 7.2 Hz, $H_{2'',6''}$), 8.657(1H, d, J = 4.0 Hz, H_5), 8.744(1H, d, J = 9.2 Hz, $H_{6'}$). ^{13}C NMR (100 MHz, DMSO-d_6) δ/ppm: 114.28(CH C_6), 116.99($C_{quaternary}$ $C_{4''}$), 119.96(CH C_8), 120.63(CH $C_{5'}$), 121.13(CH $C_{3'}$), 121.39(CH C_7), 122.04(CH C_5), 122.72($C_{quaternary}$ C_9), 128.73($C_{quaternary}$ C_3), 129.33(CH $C_{2'',6''}$), 129.57(CH $C_{3'',5''}$), 134.87($C_{quaternary}$ $C_{1''}$), 136.41(CH $C_{4'}$), 136.80($C_{quaternary}$ C_1), 149.16(CH $C_{6'}$), 154.92($C_{quaternary}$ $C_{2'}$). FT-IR (400-4000 cm^{-1}): ν(C–H)$_{stretching}$; 3024 cm^{-1}, ν(C=N)$_{stretching}$; 1581 cm^{-1}, ν(C=C)$_{stretching}$; 1519, 1473 cm^{-1}, ν(C–N)$_{stretching}$; 1218 cm^{-1}, ν(C–Cl)$_{stretching}$; 1095 cm^{-1}, Mass (m/z): 306 $[M]^+$, 308 $[M+2]^+$.

4.3.5. 3-(4-Bromophenyl)-1-(pyridin-2-yl)imidazo[1,5-a]pyridine (L^5)

Synthesized using 2,2′-dipyridylketone with p-bromobenzaldehyde as given procedure. Colour: yellow, Yield: 85%, mol. wt.: 350.22 g/mol, m. p.: 172.03 °C, Anal. Calc. (%) For $C_{18}H_{12}BrN_3$: C, 61.73; H, 3.45; N, 12.00 Found (%): C, 61.62; H, 3.33; N, 11.55. ^{1}H NMR (400 MHz, DMSO-d_6) δ/ppm: 6.708(1H, t, J = 6.0 Hz, H_6), 6.949–6.990(1H, m, H_7), 7.117–7.150(1H, m, $H_{5'}$), 7.694–7.120(2H, m, $H_{3'',5''}$), 7.751(1H, t, J = 2.4 Hz, $H_{2'',6''}$), 7.771(1H, d, J = 1.6 Hz, $H_{3'}$), 8.23–8.26(2H, m, $H_{8,4'}$), 8.646–8.665(1H, m, H_5), 8.730(1H, t, J = 0.8 Hz, $H_{6'}$). ^{13}C NMR (100 MHz, DMSO-d_6) δ/ppm: 114.30(CH C_6), 119.95(CH C_8) 120.60(CH $C_{5'}$), 121.12(CH $C_{3'}$), 122.02(CH C_7), 122.92($C_{quaternary}$ $C_{4''}$), 129.13($C_{quaternary}$ C_9), 129.81(CH C_5), 130.44($C_{quaternary}$ $C_{1''}$), 132.18(CH $C_{2'',6''}$), 136.29(CH $C_{3'',5''}$), 136.97(CH $C_{4'}$), 139.58($C_{quaternary}$ C_3), 144.19($C_{quaternary}$ C_1), 149.04(CH $C_{6'}$), 154.89($C_{quaternary}$ $C_{2'}$). FT-IR (400-4000 cm^{-1}): ν(C–H)$_{stretching}$; 3001 cm^{-1}, ν(C=N)$_{stretching}$; 1581 cm^{-1}, ν(C=C)$_{stretching}$; 1512, 1473 cm^{-1}, ν(C–N)$_{stretching}$; 1218 cm^{-1}, ν(C–Br)$_{stretching}$; 1072 cm^{-1}, Mass (m/z): 350 $[M]^+$, 352 $[M+2]^+$.

4.4. Synthesis, spectral and analytical data of Au(III) complexes

The methanolic solution of $HAuCl_4 3H_2O$ (2.5 mmol) was heated for 10 min to activate metal. Then dropwise a methanolic solution of imidazo [1,2-*a*]pyridine derivatives (2.5 mmol) was added and the reaction mixture was refluxed for 2 h at 60 °C. The obtained orange precipitate was filtered then washed with water and ether.

4.4.1. Complex-I

Colour: orange, Yield: 65%, mol. wt.: 574.64 g/mol, m. p.: >300 °C, Anal. Calc. (%) For $C_{18}H_{13}AuCl_3N_3$: C, 37.62; H, 2.28; N, 7.31 Found (%): C, 37.79; H, 2.32; N, 7.36. Λm (1 mmol L^{-1} in DMSO): 93 υ cm^2 mole^{-1}. ^{1}H NMR (400 MHz, DMSO-d_6) δ/ppm: 6.859(1H, t, J = 6.8 Hz, $H_{4''}$), 7.089 (1H, dd, J = 2.4, 6.4 Hz, H_8), 7.148 (1H, t, J = 6.0 Hz, $H_{3''}$), 7.250 (1H, dd, J = 2.4, 5.2 Hz, $H_{5''}$), 7.758–7.857 (3H, m, $H_{6,2'',6''}$), 8.330 (1H, d, J = 8.0 Hz, $H_{5'}$), 8.515 (1H, d, J = 8.0 Hz, $H_{3'}$), 8.683 (2H, d, J = 4.0 Hz, $H_{7,6'}$), 8.801 (1H, d, J = 8.8 Hz, H_5), 10.062 (1H, d, J = 7.2 Hz, $H_{4'}$), ^{13}C NMR (100 MHz, DMSO-d_6) δ/ppm: 114.34(CH C_6), 120.04(CH C_8), 120.62(CH $C_{3'}$), 121.06(CH C_7), 121.76(CH $C_{5'}$), 122.22(CH C_5), 122.30(CH $C_{4''}$), 126.28(CH $C_{3'',5''}$), 130.71($C_{quaternary}$ $C_{1''}$), 132.07($C_{quaternary}$ C_1), 136.23(CH $C_{2'',6''}$), 136.49(CH $C_{4'}$), 148.15(CH $C_{6'}$), 149.01($C_{quaternary}$ C_3), 151.07($C_{quaternary}$ C_9), 155.01($C_{quaternary}$ $C_{2'}$). FT-IR (400-4000 cm^{-1}): ν(C–H)$_{stretching}$; 3070 cm^{-1}, ν(C=N)$_{stretching}$; 1650 cm^{-1}, ν(C=C)$_{stretching}$; 1519, 1458 cm^{-1}, ν(C–N)$_{stretching}$; 1218 cm^{-1}, ν(Au–N)$_{stretching}$; 516 cm^{-1}, Mass (m/z): 538 $[M]^+$, 540 $[M+2]^+$, 542 $[M+4]^+$.

4.4.2. Complex-II

Colour: orange, Yield: 62%, mol. wt.: 574.64 g/mol, m. p.: >300 °C, Anal. Calc. (%) For $C_{18}H_{13}AuCl_3N_3$: C, 37.62; H, 2.28; N, 7.31 Found (%):

C, 37.76; H, 2.16; N, 7.40. Λm (1 mmol L^{-1} in DMSO): 91 υ cm^2 $mole^{-1}$. ^{1}H NMR (400 MHz, DMSO-d_6) δ/ppm: 7.099(1H, t, J = 6.8 Hz, H_8), 7.452(1H, dd, J =2.4, 6.8 Hz, $H_{4''}$), 7.653(4H, m, $H_{3'',5'',2'',6''}$), 7.963(2H, d, J = 1.6 Hz, $H_{6,5'}$), 8.430 (2H, t, J =7.6 Hz, $H_{3',6'}$), 8.826 (1H, d, J = 8.0 Hz, H_8), 8.658 (2H, d, J =6.4 Hz, $H_{5,4'}$). ^{13}C NMR (100 MHz, DMSO-d_6) δ/ppm: 116.07(CH C_6), 118.90(CH C_8), 122.43(CH $C_{3'}$), 122.61(CH C_7), 124.82(CH $C_{5'}$), 125.59($C_{quaternary}$ $C_{1''}$), 126.73(CH C_5), 128.60(CH $C_{quaternary}$ C_1), 129.23(CH $C_{4''}$), 129.64(CH $C_{2'',6''}$), 130.47(CH $C_{3'',5''}$), 132.60($C_{quaternary}$ C_3), 139.06(CH $C_{4'}$), 140.49($C_{quaternary}$ C_9), 144.54(CH $C_{6'}$), 150.79($C_{quaternary}$ $C_{2'}$). FT-IR (400-4000 cm^{-1}): ν(C–H)$_{stretching}$; 3024 cm^{-1}, ν(C=N)$_{stretching}$; 1604 cm^{-1}, ν(C=C)$_{stretching}$; 1504, 1434 cm^{-1}, ν(C–N)$_{stretching}$; 1257 cm^{-1}, ν(Au–N)$_{stretching}$; 563 cm^{-1}, Mass (m/z): 538 $[M]^+$, 540 $[M+2]^+$, 542 $[M+4]^+$.

4.4.3. Complex-III

Colour: orange, Yield: 57%, mol. wt.: 588.7 g/mol, m. p.: >300 °C, Anal. Calc. (%) For $C_{19}H_{15}AuCl_3N_3$: C, 38.77; H, 2.57; N, 7.14 Found (%): C, 38.80; H, 2.56; N, 7.18. Λm (1 mmol L^{-1} in DMSO): 99 υ cm^2 $mole^{-1}$. ^{1}H NMR (400 MHz, DMSO-d_6) δ/ppm: 2.454(3H, s, CH_3), 7.110 (1H, t, J = 7.6 Hz, H_8), 7.473(3H, t, J = 8.0 Hz, $H_{3'',5'',5'}$), 7.704(1H, t, J = 6.0 Hz, H_6), 7.828(2H, d, J = 8.0 Hz, $H_{2'',6''}$), 8.451(2H, dd, J = 8.4, 9.6 Hz, $H_{3',6'}$), 8.554(1H, t, J = 8.4 Hz, H_7), 8.647(2H, t, J = 7.2 Hz, $H_{5,4'}$). ^{13}C NMR (100 MHz, DMSO-d_6) δ/ppm: 21.55(CH_3), 116.15(CH C_6), 118.63(CH C_8), 121.13($C_{quaternary}$ $C_{1''}$), 122.70(CH $C_{3'}$), 125.03(CH C_7), 125.52($C_{quaternary}$ $C_{4''}$), 127.15(CH $C_{5'}$), 129.21(CH C_5), 130.20(CH $C_{2'',6''}$), 132.81($C_{quaternary}$ C_1), 140.39($C_{quaternary}$ C_3), 140.90($C_{quaternary}$ C_9), 142.54(CH $C_{3'',5''}$), 145.66(CH $C_{4',6'}$), 146.16($C_{quaternary}$ $C_{2'}$). FT-IR (400-4000 cm^{-1}): ν(C–H)$_{stretching}$; 3093 cm^{-1}, ν(C=N)$_{stretching}$; 1612 cm^{-1}, ν(C=C)$_{stretching}$; 1519, 1488 cm^{-1}, ν(C–N)$_{stretching}$; 1249 cm^{-1}, ν(Au–N)$_{stretching}$; 524 cm^{-1}, Mass (m/z): 552 $[M]^+$, 554 $[M+2]^+$, 556 $[M+4]^+$.

4.4.4. Complex-IV

Colour: orange, Yield: 68%, mol. wt.: 609.1 g/mol, m. p.: >300 °C, Anal. Calc. (%) For $C_{18}H_{12}AuCl_4N_3$: C, 35.50; H, 1.99; N, 6.90 Found (%): C, 35.91; H, 2.03; N, 6.91. Λm (1 mmol L^{-1} in DMSO): 95 υ cm^2 $mole^{-1}$. ^{1}H NMR (400 MHz, DMSO-d_6) δ/ppm: 7.082(1H, t, J = 7.6 Hz, H_8), 7.422(1H, t, J = 8.0 Hz, H_6), 7.635(1H, s, $H_{5'}$), 7.720(2H, d, J = 8.0 Hz, $H_{3'',5''}$), 7.977(2H, d, J = 7.2 Hz, $H_{2'',6''}$), 8.377(2H, t, J = 7.2 Hz, $H_{3'}$), 8.472(2H, t, J = 6.8 Hz, $H_{7,6'}$), 8.647(2H, t, J = 7.6 Hz, $H_{5,4'}$). ^{13}C NMR (100 MHz, DMSO-d_6) δ/ppm: 116.03(CH C_6), 119.05(CH C_8), 122.24(CH $C_{3'}$), 122.57($C_{quaternary}$ $C_{1''}$), 124.76(CH $C_{7,5'}$), 126.48(CH C_5), 127.66($C_{quaternary}$ $C_{4''}$), 129.69(CH $C_{2'',6''}$), 130.90(CH $C_{3'',5''}$), 132.55($C_{quaternary}$ C_1), 134.93($C_{quaternary}$ C_3), 139.18($C_{quaternary}$ C_9), 143.73(CH $C_{6'}$), 147.27(CH $C_{4'}$), 150.55($C_{quaternary}$ $C_{2'}$). FT-IR (400-4000 cm^{-1}): ν(C–H)$_{stretching}$; 3085 cm^{-1}, ν(C=N)$_{stretching}$; 1604 cm^{-1}, ν(C=C)$_{stretching}$; 1542, 1496 cm^{-1}, ν(C–N)$_{stretching}$; 1242 cm^{-1}, ν(C–Cl)$_{stretching}$; 1087 cm^{-1}, ν(Au–N)$_{stretching}$; 555 cm^{-1}, Mass (m/z): 572 $[M]^+$, 574 $[M+2]^+$, 576 $[M+4]^+$, 578 $[M+6]^+$.

4.4.5. Complex-V

Colour: orange, Yield: 53%, mol. wt.: 653.5 g/mol, m. p.: >300 °C, Anal. Calc. (%) For $C_{18}H_{12}AuCl_3BrN_3$: C, 33.08; H, 1.85; N, 6.43 Found (%): C, 33.15; H, 1.90; N, 6.45. Λm (1 mmol L^{-1} in DMSO): 101 υ cm^2 $mole^{-1}$. ^{1}H NMR (400 MHz, DMSO-d_6) δ/ppm: 7.099(1H, s, H_8), 7.439(1H, s, H_6), 7.659(1H, s, $H_{5'}$), 7.869(4H, s, $H_{2'',3'',5'',6''}$), 8.433(3H, s, $H_{7,3',6'}$), 8.659(2H, s, $H_{5,4'}$). ^{13}C NMR (100 MHz, DMSO-d_6) δ/ppm: 116.23(CH C_6), 118.88(CH C_8), 122.55(CH $C_{3'}$), 122.83 (CH C_7), 123.79($C_{quaternary}$ $C_{4''}$), 124.63($C_{quaternary}$ $C_{1''}$), 125.03(CH $C_{5'}$), 126.95(CH C_5), 127.96($C_{quaternary}$ C_1), 131.23(CH $C_{2'',6''}$), 132.70(CH $C_{3'',5''}$), 139.47($C_{quaternary}$ C_3), 144.99(CH $C_{4',6'}$), 146.89($C_{quaternary}$ C_9), 150.27($C_{quaternary}$ $C_{2'}$). FT-IR (400-4000 cm^{-1}): ν(C–H)$_{stretching}$; 3024 cm^{-1}, ν(C=N)$_{stretching}$; 1604 cm^{-1}, ν(C=C)$_{stretching}$; 1512, 1434 cm^{-1}, ν(C–N)$_{stretching}$; 1249 cm^{-1}, ν(C–Br)$_{stretching}$; 1064 cm^{-1}, ν(Au–N)$_{stretching}$; 555 cm^{-1}, Mass (m/z): 616 $[M]^+$, 618 $[M+2]^+$, 620 $[M+4]^+$, 622 $[M+6]^+$.

4.5. In vitro antibacterial activity

The *in vitro* antibacterial activity of imidazo [1,2-*a*]pyridine derivatives and synthesized Au(III) complexes was performed against two Gram positive: *Staphylococcus aureus*, *Bacillus subtilis* and three Gram negative: *Serratia marcescens, Escherichia coli, Pseudomonas aeruginosa* microorganisms. The experiment was performed according to the literature procedure [22].

4.6. DNA interaction study by absorption titration

UV visible absorption titration is carried out using a known concentration of HS-DNA (0–100 μM) in phosphate buffer (5 mM Tris/HCl, pH 7.5) and synthesized complexes (5 μM in DMSO). HS-DNA was dissolved in phosphate buffer and concentration of DNA is measured at 260 nm wavelength (ε = 12858 cm^{-1}). The experiment was carried out according to our previously published literature [23].

4.7. DNA interaction study by viscosity measurement

The hydrodynamic volume measurement study was carried out using an Ubbelohed viscometer kept under the thermostatic bath at constant temperature of 27 ± 0.1 °C. The experiment was carried out according to the literature [24].

4.8. Molecular docking

To determine the theoretical binding energy of synthesized compounds to DNA, docking study was performed using HEX 6.0 software. The. pdb files of complex coordinates were obtained by converting their. mol file using CHIMERA 1.5.1 software. The structure of B-DNA (1 BNA: 5′-D (*CP*GP*CP*GP*AP*TP*TP*CP*GP*CP*G)-3′) obtained from the Protein Data Bank (http://www.rcsb.org/pdb). All solvents were removed before docking. Grid dimension 0.6 with FFT mode 3D and correlation type shape only were used. The other parameters kept at their default values.

4.9. In vitro and in vivo cytotoxicity

In vitro cytotoxicity was performed according to our previously published literature [25]. Data were analyzed by simple logit method to determine the LC_{50} values, in which the log of the concentration of samples was plotted against the percentage of mortality of nauplii. The *in vivo* cytotoxicity was performed according to literature using *S. Pombe* cells [25].

4.10. Single cell gel electrophoresis

In this study, the yeast cells were kept in ice-chilled PBS to prepare a single cell suspension and were used in minigel, which was made on the microscopic slides by using 1% normal melting point (NMP) agarose as the 1st layer. A 110 μL NMP was poured on the slide and then 2nd layer was made with the mixture of yeast cell suspension (10 μL) and 0.5% low melting point (LMP) agarose (65 μL). This was poured over the 1st layer and exposed slides were submerged (after solidification) in chilled lysing solution (2.5 M NaCl, 100 mM Na_2EDTA, 10 mM Tris HCl, 1% Triton X-100, 10% DMSO, pH 10) overnight at 4 °C in dark condition. After lysis, the slides were transferred to a jar containing alkaline electrophoresis buffer (1 mM Na_2EDTA, 300 mM NaOH, pH > 13) for 20 min at 4 °C [26]. All slides were transferred to an electrophoresis tank containing the same alkaline buffer and subjected to an electric field of 0.86 V/cm for 20 min at 4 °C. After electrophoresis, all the slides containing minigels were neutralized in buffer (0.4 M Tris HCl, pH 7.5) and finally rinsed in double distilled water. The staining of DNA was done by ethidium bromide (25 μL per slide) for 20 min. The analysis of DNA damage, especially tail moment was visualized under a fluorescence microscope equipped with

excitation filter BP 515–560 nm with barrier filter LP 590 nm and recorded.

4.11. MTT assay

The half maximal inhibitory concentration (IC_{50}) value of Au(III) complexes was determined by MTT assay, in which A549 cells were treated with a series of concentrations (control, DMSO, 10, 25, 50, 100, 250, 500 μg/mL) of complexes for 24 h. The cells were washed twice with DPBS and incubated with 0.5 mg/mL MTT solution for 4 h at 37 °C. Thereafter, 0.1 mL of SDS-HCl (10% SDS in 0.01 M HCl) was added to each well, mixed thoroughly and allowed for incubation in the dark for 20 min at 37 °C. Finally, the absorbance of each well was recorded at 570 nm with a reference wavelength of 650 nm using a multimode micro plate reader (Spectra Max M2e, Molecular devices, USA). The results are represented in terms of percentage inhibition of cell proliferation compared to that of vehicle control.

Declarations

Author contribution statement

Mohan Patel, Darshana Kanthecha, Bhupesh Bhatt: Conceived and designed the experiments; Performed the experiments; Analyzed and interpreted the data; Contributed reagents, materials, analysis tools or data; Wrote the paper.

Funding statement

This work was supported by U.G.C. New Delhi (UGC-BSR grant No. C/2013/BSR/Chemistry/1573).

Competing interest statement

The authors declare no conflict of interest.

Additional information

No additional information is available for this paper.

Acknowledgements

The authors thankful to the Head, Department of Chemistry, Sardar Patel University, Vallabh Vidyanagar, Gujarat, India, for providing the laboratory facilities, SAIF Panjab university for C, H, N and ESI-MS analysis, DST PURSE Sardar Patel University, Vallabh Vidyanagar for LC-MS analysis.

References

[1] L.H. Hurley, DNA and its associated processes as targets for cancer therapy, Nat. Rev. Canc. 2 (2002) 188.

[2] (a) S. Nobili, E. Mini, I. Landini, C. Gabbiani, A. Casini, L. Messori, Gold compounds as anticancer agents: chemistry, cellular pharmacology, and preclinical studies, Med. Res. Rev. 30 (2010) 550–580;
(b) G. Sava, A. Bergamo, P.J. Dyson, Metal-based antitumour drugs in the post-genomic era: what comes next? Dalton Trans. 40 (2011) 9069–9075;
(c) M. Wenzel, A. De Almeida, E. Bigaeva, P. Kavanagh, M. Picquet, P. Le Gendre, E. Bodio, A. Casini, New luminescent polynuclear metal complexes with anticancer properties: Toward structure–activity, Inorg. Chem. 55 (2016) 2544–2557;
(d) J. Du, Y. Wei, Y. Zhao, F. Xu, Y. Wang, W. Zheng, Q. Luo, M. Wang, F. Wang, A photoactive platinum(IV) anticancer complex inhibits thioredoxin–thioredoxin reductase system activity by induced oxidization of the protein, Inorg. Chem. 57 (2018) 5575–5584.

[3] B. Rosenberg, L. Vancamp, J.E. Trosko, V.H. Mansour, Platinum compounds: a new class of potent antitumour agents, Nature 222 (1969) 385.

[4] T.C. Johnstone, K. Suntharalingam, S.J. Lippard, Third row transition metals for the treatment of cancer, Phil. Trans. R. Soc. A 373 (2015) 20140185.

[5] (a) V. Cepeda, M.A. Fuertes, J. Castilla, C. Alonso, C. Quevedo, J.M. Pérez, Biochemical mechanisms of cisplatin cytotoxicit, Anti Cancer Agents Med. Chem. 7 (2007) 3–18;
(b) C. Billecke, S. Finniss, L. Tahash, C. Miller, T. Mikkelsen, N.P. Farrell, O. Bögler, Polynuclear platinum anticancer drugs are more potent than cisplatin and induce cell cycle arrest in glioma, Neuro Oncol. 8 (2006) 215–226.

[6] L. Galluzzi, L. Senovilla, I. Vitale, J. Michels, I. Martins, O. Kepp, M. Castedo, G. Kroemer, Molecular mechanisms of cisplatin resistance, Oncogene 31 (2012) 1869.

[7] (a) F. Barragán, D. Carrion-Salip, I. Gómez-Pinto, A. González-Cantó, P.J. Sadler, R. de Llorens, V. Moreno, C. González, A. Massaguer, V. Marchán, Somatostatin subtype-2 receptor-targeted metal-based anticancer complexes, Bioconjug. Chem. 23 (2012) 1838–1855;
(b) C. Santini, M. Pellei, V. Gandin, M. Porchia, F. Tisato, C. Marzano, Advances in copper complexes as anticancer agents, Chem. Rev. 114 (2014) 815–862;
(c) T. McGivern, S. Afsharpour, C. Marmion, Copper complexes as artificial DNA metallonucleases: from Sigman's reagent to next generation anti-cancer agent? Inorg. Chim. Acta 472 (2018) 12–39;
(d) P. Zhang, P.J. Sadler, Advances in the design of organometallic anticancer complexes, J. Organomet. Chem. 839 (2017) 5–14;
(e) D.L. Ma, H.Z. He, K.H. Leung, D.S.H. Chan, C.H. Leung, Bioactive luminescent transition-metal complexes for biomedical applications, Angew. Chem. Int. Ed. 52 (2013) 7666–7682;
(f) L. Salassa, Polypyridyl metal complexes with biological activity, Eur. J. Inorg. Chem. 2011 (2011) 4931–4947;
(g) D. Hegde, S. Dodamani, V. Kumbar, S. Jalalpure, K.B. Gudasi, Synthesis, crystal structure, DNA interaction and anticancer evaluation of pyruvic acid derived hydrazone and its transition metal complexes, Appl. Organomet. Chem. 31 (2017) 3851;
(h) W.H. Mahmoud, F.N. Sayed, G.G. Mohamed, Azo dye with nitrogen donor sets of atoms and its metal complexes: Synthesis, characterization, DFT, biological, anticancer and Molecular docking studies, Appl. Organomet. Chem. 32 (2018) 4347;
(i) P. Zhang, P.J. Sadler, Redox-active metal complexes for anticancer therapy, Eur. J. Inorg. Chem. 2017 (2017) 1541–1548;
(j) E. Alessio, Z. Guo, Metal anticancer complexes–activity, mechanism of action, future perspectives, Eur. J. Inorg. Chem. 2017 (2017) 1539–1540;
(k) M.M. Abd-Elzaher, S.A. Moustafa, A.A. Labib, H.A. Mousa, M.M. Ali, A.E. Mahmoud, Synthesis, characterization and anticancer studies of ferrocenyl complexes containing thiazole moiety, Appl. Organomet. Chem. 26 (2012) 230–236;
(l) H.A. El-Ghamry, S.K. Fathalla, M. Gaber, Synthesis, structural characterization and molecular modelling of bidentate azo dye metal complexes: DNA interaction to antimicrobial and anticancer activities, Appl. Organomet. Chem. 32 (2018) 4136;
(m) D. İnci, R. Aydın, H. Huriyet, Y. Zorlu, N. Çinkılıç, Newly synthesized Cu(II) pyrazino [2, 3-f][1, 10] phenanthroline complexes as potential anticancer candidates, Appl. Organomet. Chem. 32 (2018) 4309;
(n) F. Ponte, I. Ritacco, G. Mazzone, N. Russo, E. Sicilia, Theoretical determination of the aquation reaction mechanism of cyclometalated benzimidazole Ru(II) and Ir(III) anticancer complexes, Inorg. Chim. Acta 470 (2018) 325–330;
(o) A. Erxleben, Transition metal salen complexes in bioinorganic and medicinal chemistry, Inorg. Chim. Acta 472 (2018) 40–57;
(p) Ö. Tarı, F. Gümüş, L. Açık, B. Aydın, Synthesis, characterization and DNA binding studies of platinum (II) complexes with benzimidazole derivative ligands, Bioorg. Chem. 74 (2017) 272–283;
(q) L.H. Abdel-Rahman, A.M. Abu-Dief, R.M. El-Khatib, S.M. Abdel-Fatah, Some new nano-sized Fe (II), Cd (II) and Zn (II) Schiff base complexes as precursor for metal oxides: sonochemical synthesis, characterization, DNA interaction, in vitro antimicrobial and anticancer activities, Bioorg. Chem. 69 (2016) 140–152;
(r) P.A. Vekariya, P.S. Karia, B.S. Bhatt, M.N. Patel, Half sandwich rhodium(III) and iridium(III) complexes as cytotoxic and metallonuclease agents, Appl. Biochem. Biotechnol. 187 (2) (2019) 556–569;
(s) K.P. Thakor, M.V. Lunagariya, B.S. Bhatt, M.N. Patel, Synthesis, characterization and biological applications of some substituted pyrazoline based palladium (II) compounds, Appl. Organomet. Chem. 32 (2018) e4523;
(t) C. Saturnino, M. Napoli, G. Paolucci, M. Bortoluzzi, A. Popolo, A. Pinto, P. Longo, Synthesis and cytotoxic activities of group 3 metal complexes having monoanionic tridentate ligands, Eur. J. Med. Chem. 45 (2010) 4169–4174;
(u) A.M. Gouda, H.A. El-Ghamry, T.M. Bawazeer, T.A. Farghaly, A.N. Abdalla, A. Aslam, Antitumor activity of pyrrolizines and their Cu(II) complexes: Design, synthesis and cytotoxic screening with potential apoptosis-inducing activity, Eur. J. Med. Chem. 145 (2018) 350–359;
(v) M.R.E.S. Aly, H.H.A.E.R. Fodah, S.Y. Saleh, Antiobesity, antioxidant and cytotoxicity activities of newly synthesized chalcone derivatives and their metal complexes, Eur. J. Med. Chem. 76 (2014) 517–530.

[8] (a) S. Tian, F.-M. Siu, S.C. Kui, C.-N. Lok, C.-M. Che, Anticancer gold(I)–phosphine complexes as potent autophagy-inducing agents, Chem. Commun. 47 (2011) 9318–9320;
(b) M. Serratrice, F. Edafe, F. Mendes, R. Scopelliti, S.M. Zakeeruddin, M. Grätzel, I. Santos, M.A. Cinellu, A. Casini, Cytotoxic gold compounds: synthesis, biological characterization and investigation of their inhibition properties of the zinc finger protein PARP-1, Dalton Trans. 41 (2012) 3287–3293;
(c) T. Zou, J.J. Zhang, B. Cao, K.C. Tong, C.N. Lok, C.M. Che, Deubiquitinases as anticancer targets of gold complexes, Isr. J. Chem. 56 (2016) 825–833;
(d) O. Dada, G. Sánchez-Sanz, M. Tacke, X. Zhu, Synthesis and anticancer activity of novel NHC-gold(I)-sugar complexes, Tetrahedron Lett. 59 (2018) 2904–2908;
(e) F. Hackenberg, H. Müller-Bunz, R. Smith, W. Streciwilk, X. Zhu, M. Tacke, Novel ruthenium(II) and gold(I) NHC complexes: synthesis, characterization, and evaluation of their anticancer properties, Organometallics 32 (2013) 5551–5560;

(f) M. Fereidoonnezhad, H.R. Shahsavari, E. Lotfi, M. Babaghasabha, M. Fakhri, Z. Faghih, Z. Faghih, M. Hassan Beyzavi, (Benzyl isocyanide) gold (I) pyrimidine-2-thiolate complex: Synthesis and biological activity, Appl. Organomet. Chem. 32 (2018) 4200;
(g) A.C. Goncalves, Z.A. Carneiro, C.G. Oliveira, A. Danuello, W. Guerra, R.J. Oliveira, F.B. Ferreira, L.L. Veloso-Silva, F.A. Batista, J.C. Borges, Pt II, Pd II and Au III complexes with a thiosemicarbazone derived from diacethylmonooxime: Structural analysis, trypanocidal activity, cytotoxicity and first insight into the antiparasitic mechanism of action, Eur. J. Med. Chem. 141 (2017) 615–631.

[9] (a) A.A. Seliman, M. Altaf, A.T. Onawole, A. Al-Saadi, S. Ahmad, A. Alhoshani, G. Bhatia, A.A. Isab, Synthesis, X-ray structure and cytotoxicity evaluation of carbene-based gold (I) complexes of selenones, Inorg. Chim. Acta 476 (2018) 46–53;
(b) M.N. Patel, B.S. Bhatt, P.A. Dosi, DNA binding, cytotoxicity and DNA cleavage promoted by gold(III) complexes, Inorg. Chem. Commun. 29 (2013) 190–193;
(c) M.N. Patel, B.S. Bhatt, P.A. Dosi, Synthesis and evaluation of gold(III) complexes as efficient DNA binders and cytotoxic agents, Spectrochim. Acta A 110 (2013) 20–27;
(d) C. Martín-Santos, E. Michelucci, T. Marzo, L. Messori, P. Szumlas, P.J. Bednarski, R. Mas-Ballesté, C. Navarro-Ranninger, S. Cabrera, J. Alemán, Gold(III) complexes with hydroxyquinoline, aminoquinoline and quinoline ligands: synthesis, cytotoxicity, DNA and protein binding studies, J. Inorg. Biochem. 153 (2015) 339–345;
(e) L. Ortego, F. Cardoso, S. Martins, M.F. Fillat, A. Laguna, M. Meireles, M.D. Villacampa, M.C. Gimeno, Strong inhibition of thioredoxin reductase by highly cytotoxic gold (I) complexes. DNA binding studies, J. Inorg. Biochem. 130 (2014) 32–37.

[10] (a) K.P. Thakor, M.V. Lunagariya, B.S. Bhatt, M.N. Patel, Fluorescence and absorption studies of DNA–Pd (II) complex interaction: Synthesis, spectroanalytical investigations and biological activities, Luminescence 34 (2019) 113–124;
(b) L. Ronconi, P.J. Sadler, Using coordination chemistry to design new medicines, Coord. Chem. Rev. 251 (2007) 1633–1648.

[11] (a) J.A. War, S.K. Srivastava, S.D. Srivastava, Synthesis and DNA-binding study of imidazole linked thiazolidinone derivatives, Luminescence 32 (2017) 104–113;
(b) Y.-L. Fan, X.-H. Jin, Z.-P. Huang, H.-F. Yu, Z.-G. Zeng, T. Gao, L.-S. Feng, Recent advances of imidazole-containing derivatives as anti-tubercular agents, Eur. J. Med. Chem. 150 (2018) 347–365;
(c) M.A. Ewida, D.A.A. El Ella, D.S. Lasheen, H.A. Ewida, Y.I. El-Gazzar, H.I. El-Subbagh, Imidazo [2', 1': 2, 3] thiazolo [4, 5-d] pyridazinone as a new scaffold of DHFR inhibitors: Synthesis, biological evaluation and molecular modeling study, Bioorg. Chem. 80 (2018) 11–23.

[12] M.N. Patel, B.S. Bhatt, P.A. Dosi, Topoisomerase inhibition, nucleolytic and electrolytic contribution on DNA binding activity exerted by biological active analogue of coordination compounds, Appl. Biochem. Biotechnol. 166 (2012) 1949–1968.

[13] R. Gup, O. Erer, N. Dilek, One-pot synthesis of a new 2-substituted 1, 2, 3-triazole 1-oxide derivative from dipyridyl ketone and isonitrosoacetophenone hydrazone: Nickel(II) complex, DNA binding and cleavage properties, Bioorg. Chem. 71 (2017) 325–334.

[14] J.-H. Shi, T.-T. Liu, M. Jiang, J. Chen, Q. Wang, Characterization of interaction of calf thymus DNA with gefitinib: spectroscopic methods and molecular docking, J. Photochem. Photobiol. B Biol. 147 (2015) 47–55.

[15] M. Sirajuddin, S. Ali, A. Badshah, Drug–DNA interactions and their study by UV–Visible, fluorescence spectroscopies and cyclic voltammetry, J. Photochem. Photobiol. B Biol. 124 (2013) 1–19.

[16] S.S. Al-Jaroudi, M. Altaf, A.A. Seliman, S. Yadav, F. Arjmand, A. Alhoshani, H.M. Korashy, S. Ahmad, A.A. Isab, Synthesis, characterization, in vitro cytotoxicity and DNA interaction study of phosphane gold(I) complexes with dithiocarbamate ligands, Inorg. Chim. Acta 464 (2017) 37–48.

[17] Y.-J. Schneider, R. Baurain, A. Zenebergh, A. Trouet, DNA-binding parameters of daunorubicin and doxorubicin in the conditions used for studying the interaction of anthracycline-DNA complexes with cells in vitro, Cancer Chemother. Pharmacol. 2 (1979) 7–10.

[18] (a) C.N. N'Soukpoé-Kossi, C. Descôteaux, É. Asselin, H.-A. Tajmir-Riahi, G. Bérubé, DNA interaction with novel antitumor estradiol–platinum(II) hybrid molecule: a comparative study with cisplatin drug, DNA Cell Biol. 27 (2007) 101–107;
(b) M.J. Waring, Complex formation between ethidium bromide and nucleic acids, J. Mol. Biol. 13 (1965) 269–282.

[19] B. Meyer, N. Ferrigni, J. Putnam, L. Jacobsen, D. Nichols, J.L. McLaughlin, Brine shrimp: a convenient general bioassay for active plant constituents, Planta Med. 45 (1982) 31–34.

[20] J.V. Mehta, S.B. Gajera, P. Thakor, V.R. Thakkar, M.N. Patel, Patel, Synthesis of 1, 3, 5-trisubstituted pyrazoline derivatives and their applications, RSC Adv. 5 (2015) 85350–85362.

[21] D.N. Kanthecha, D.B. Raval, V.R. Thakkar, M.N. Patel, Biological significance of hetero-scaffolds based gold(III) complexes, Acta Chim. Slov. 65 (2018) 333–343.

[22] (a) P.A. Vekariya, P.S. Karia, J.V. Vaghasiya, S. Soni, E. Suresh, M.N. Patel, Evolution of rhodium(III) and iridium(III) chelates as metallonucleases, Polyhedron 110 (2016) 73–84;
(b) L.H. Abdel-Rahman, N.M. Ismail, M. Ismael, A.M. Abu-Dief, E.A.-H. Ahmed, Synthesis, characterization, DFT calculations and biological studies of Mn(II), Fe(II), Co(II) and Cd(II) complexes based on a tetradentate ONNO donor Schiff base ligand, J. Mol. Struct. 1134 (2017) 851–862.

[23] P.A. Vekariya, P.S. Karia, B.S. Bhatt, M.N. Patel, Effect of substituents on the biological activities of piano stool η5-cyclopentadienyl Rh(III) and Ir(III) complexes, J. Inorg. Organomet. Polym. Mater. 28 (2018) 2749–2758.

[24] (a) L.H.A. Rahman, A.M. Abu-Dief, N.A. Hashem, A.A. Seleem, Recent advances in synthesis, characterization and biological activity of nano sized Schiff base amino acid M(II) complexes, Int. J. Nano. Chem 1 (2015) 79–95;
(b) L.H. Abdel-Rahman, A.M. Abu-Dief, E.F. Newair, S.K. Hamdan, Some new nano-sized Cr(III), Fe(II), Co(II), and Ni(II) complexes incorporating 2-((E)-(pyridine-2-ylimino) methyl) napthalen-1-ol ligand: structural characterization, electrochemical, antioxidant, antimicrobial, antiviral assessment and DNA interaction, J. Photochem. Photobiol. B Biol. 160 (2016) 18–31.

[25] K.P. Thakor, M.V. Lunagariya, B.S. Bhatt, M.N. Patel, Fluorescence and absorption titrations of bio-relevant imidazole based organometallic Pd(II) complexes with DNA: synthesis, characterization, dna interaction, antimicrobial, cytotoxic and molecular docking studies, J. Inorg. Organomet. Polym. Mater. (2019) 1–12.

[26] P. Banerjee, S.N. Talapatra, N. Mandal, G. Sundaram, A. Mukhopadhyay, D. Chattopadhyay, S.K. Banerjee, Genotoxicity study with special reference to DNA damage by comet assay in fission yeast, Schizosaccharomyces pombe exposed to drinking water, Food Chem. Toxicol. 46 (2008) 402–407.